A R C H I V E S O F M E T A L L U R G Y A N D M A T E R I A L S
Volume 59 2014 Issue 4
DOI: 10.2478/amm-2014-0236

D. KALISZ*, P.L. ŻAK*

MODELING OF TiN AND Ti_2O_3 PRECIPITATES FORMATION DURING SOLIDIFICATION OF STEEL

MODELOWANIE POWSTAWANIA WYDZIELEŃ TiN I Ti_2O_3 W PROCESIE KRZEPNIĘCIA STALI

The formation of titanium nitride precipitations during solidification of steel was modeled with own computer software based on Ueshima model. A thermodynamic parameters database was worked out on the basis of literature study. Calculations were performed for two types of steel; one of them was high in titanium. The quantity of produced titanium nitrogen inclusions was calculated. The authors analyzed changes in nitrogen, titanium and oxygen content in the course of segregation of steel components on the solidification front. The influence of solidification rate on the process of precipitation formation was analyzed.

Keywords: titanium nitride, solidification of steel, segregation, computer simulation

Praca zajmuje się modelowaniem powstawania wydzieleń azotku tytanu w stali podczas krzepnięcia. Zastosowano procedurę obliczeniową z wykorzystaniem modelu Ueshima przy pomocy własnego programu komputerowego. Na podstawie studiów literaturowych przygotowano bazę danych parametrów termodynamicznych. Obliczenia wykonano dla dwóch gatunków stali, z których jeden charakteryzował się wysoką zawartością tytanu. Obliczono ilość powstających wydzieleń azotku tytanu, przeanalizowano zmiany zawartości azotu, tytanu i tlenu w wyniku procesów segregacji składników w stali na froncie krzepnięcia. Zbadano wpływ szybkości krzepnięcia na proces powstawania wydzieleń.

1. Introduction

The objective of this paper is thermodynamic analysis of TiN formation during the steel solidification process. The resulting fine (ca. 1-3 μm) and evenly distributed TiN precipitations cause that the cast steel has a fine-grain structure [1]. The research conducted by Ishikawa [2], Gregg and Bhadeshia [3] reveals that TiN inclusions can be used for making an acicular ferrite structure. It was also observed that the finest ferrite structure can be obtained using pure titanium oxides TiO_2 and Ti_2O_3. However, in reality oxides usually occur in solutions which disqualifies them as structure modifiers [1], [4-5]. Titanium nitride precipitates can be formed only when liquid steel contains appropriate amounts of titanium and nitrogen. If Ti and N content is too high, the TiN precipitations will be formed prior to the liquid steel solidification and will be removed in the course of agglomeration processes. On the other hand, when the nitrogen content is too low and the steel contains oxygen, titanium oxides will be consequently formed. The computer simulations performed by the authors [4], [5] with the use of commercial software FactSage and own computer program WYK_Stal proved that TiN is formed in the secondary refinery process which precedes casting. The microstructure of the cast steel cannot be modified with the formed TiN precipitations. The basic element of the steel structure modification is controlling the TiN inclusions formation. For doing so, it is necessary to know the state of thermodynamic equilibrium of reaction between elements of the solidifying steel. Another strongly influential factor is beneficiation of liquid steel in components dissolved at the solidification front.

2. Formation of titanium nitride and oxide precipitates

Thermodynamically, the TiN and Ti_2O_3 precipitations can be formed in liquid steel after exceeding the equilibrium value of the solubility product Q [1], [6-9]:

$$[Ti] + [N] = (TiN) \tag{1}$$

$$Q_{L(TiN)} = [\%Ti] \cdot [\%N] \tag{2}$$

$$K_{TiN} = exp\left[-\frac{\Delta G^0}{R \cdot T}\right] = \frac{a_{TiN}}{f_{Ti} \cdot f_N \cdot [\%Ti] \cdot [\%N]} = \frac{a_{TiN}}{f_{Ti} \cdot f_N \cdot Q_L} \tag{3}$$

If $a_{TiN} = 1$ and f_{Ti}, $f_N = 1$ the formula takes form:

$$K_{TiN} = exp\left[-\frac{\Delta G^0}{R \cdot T}\right] = \frac{1}{Q_L} \tag{4}$$

$$logK_{TiN} = 19790/T - 7.78 \tag{5}$$

$$\Delta G^0_{TiN} = -379000 + 149 \cdot T \tag{6}$$

$$2[Ti] + 3[O] = (Ti_2O_3) \tag{7}$$

* AGH UNIVERSITY OF SCIENCE AND TECHNOLOGY, FACULTY OF FOUNDRY ENGINEERING, AL. A. MICKIEWICZA 30, 30-059 KRAKÓW, POLAND

$$Q_{L(Ti_2O_3)} = [\%Ti]^2 \cdot [\%O]^3 \tag{8}$$

$$K_{Ti2O3} = exp\left[-\frac{\Delta G^0}{R \cdot T}\right] = \frac{a_{Ti2O3}}{f_{Ti}^2 \cdot f_O^3 \cdot [\%Ti]^2 \cdot [\%O]^3} = \frac{a_{Ti2O3}}{f_{Ti}^2 \cdot f_O^3 \cdot Q_L} \tag{9}$$

If $a_{Ti2O3} = 1$ and f_{Ti}, $f_O = 1$ the formula takes form:

$$K_{Ti2O3} = exp\left[-\frac{\Delta G^0}{R \cdot T}\right] = \frac{1}{Q_L} \tag{10}$$

$$logK_{Ti2O3} = 56060/T - -18.08 \tag{11}$$

$$\Delta G^0_{Ti2O3} = -263000 + 85.25 \cdot T \tag{12}$$

where:

$Q_{L(TiN)}, Q_{L(Ti_2O_3)}$ – solubility product,
K_{TiN} , K_{Ti2O3} – equilibrium constant for the reaction,
a_{TiN} – activity TiN,
a_{Ti2O3} – activity Ti_2O_3,
f_{Ti}, f_N, f_O – activity coefficients,
R – ideal gas constant [8.31 J/mol· K],
ΔG^0 – Gibbs energy [J/mol].

The inclusions TiN and Ti_2O_3 may be formed at an early crystallization stage, when:

$$C^t_{L(Ti)} \cdot f_{Ti} \cdot C^t_{L(N)} \cdot f_N \geqslant Q_{L(TiN)} \tag{13}$$

$$C^{t\,2}_{L(Ti)} \cdot f^2_{Ti} \cdot C^{t\,3}_{L(O)} \cdot f^3_O \geqslant Q_{L(Ti_2O_3)} \tag{14}$$

Where:

$C^t_{L(Ti)}, C^t_{L(O)}, C^t_{L(N)}$ – concentration of a components (Ti, O, N).

Dependences describing equilibrium values of solubility some products Q for selected precipitations in liquid and solid iron are presented in Table 1.

TABLE 1

Equilibrium dependences of solubility product

Inclusion	log Q	Q value at 1800 K
Ti_2O_3(s) in Fe liq. [11]	-56 060/T + 18.08	$8{,}62 \cdot 10^{-14}$
TiN (s) in Fe liq. [7]	-19 790/T + 7.781	$6{,}117 \cdot 10^{-4}$

During steel solidification all its components are segregated into solid and liquid phase. The thermodynamic criterion of inclusions formation refers to the present composition of liquid phase. The inclusions are formed, if $\Delta G < 0$ [1], [6]. The course of the liquidus and solidus lines of relevant phase diagram (iron - steel component) reveals that the component will gather in the liquid phase and the successive portions of solidifying liquid will be enriched in it, with the last portion containing highest amount of the dissolved components. In the solidifying part of the liquid, some amount of the „i" element splits into two parts: one of them enriches the liquid, the other joins the crystallization front and diffuses inside the crystal. The back diffusion results in lowering of equilibrium content of a liquid phase component. The share of back diffusion for a single liquid solution component „i" is characterized by the back diffusion α_i:

$$\alpha_i = \frac{D_i \cdot t_s}{l^2} \tag{15}$$

D_i – diffusion coefficient of a component in solid phase [m^2/s],
l – advancement of solidification front [m],
t_s – local solidification time [s],

$$t_s = \frac{T_L - T_S}{P} \tag{16}$$

where:

T_L – liquidus temperature of steel [K],
T_S – solidus temperature [K],
P – cooling rate [K/s].

Crystallization with back diffusion can be described by Wołczyński equation [12]:

$$C^*_S = k \cdot C_0 \cdot [1 + \alpha \cdot k \cdot f_S - f_S]^{\frac{k-1}{1-\alpha \cdot k}} \tag{17}$$

where:

C^*_S – concentration of a component in liquid phase,
C_0 – initial concentration of a component in liquid phase,
k – partition coefficients,
fs – fraction of solid phase.

Temperature dependences describing the diffusion coefficients and equilibrium partition coefficients are listed in Table 2.

TABLE 2

Diffusion coefficients in solid phase (ferrite D_δ, austenite D_γ) and equilibrium partition coefficients $k^{\delta/L}$ and $k^{\gamma/L}$ for steel components [11, 13-14]

Component	D_δ, $\times 10^{-4}\frac{m^2}{s}$	$k^{\delta/L}$	$D\gamma$, $\times 10^{-4}\frac{m^2}{s}$	$k^{\gamma/L}$
Mn	0.76exp(-223472/RT)	0.77	0.055exp(-59600/RT)	0.78
S	4.56exp(-214443/RT)	0.05	2.4exp(-53400/RT)	0.035
Si	8exp(-248710/RT)	0.77	0.36exp(-60100/RT)	0.52
C	0.0127exp(-81301/RT)	0.19	0.07exp(-32160/RT)	0.34
P	2.9exp(-229900/RT)	0.23	0.01exp(-43700/RT)	0.13
Al	5.9exp(-241186/RT)	0.6	5.9exp(-241186/RT)	0.6
O	0.0371exp(-96349/RT)	0.03	0.0371exp(-96349/RT)	0.03
N	0.008exp(-79078/RT)	0.25	0.9exp(-168600/RT)	0.48
Ti	3.15exp(-247693/RT)	0.38	0.15exp(-250000/RT)	0.33

During solidification, the course of temperature is influenced by: temperature dependence on diffusion coefficient in solid state for all components, cooling rate dT/dt and equilibrium division coefficient k. The solidus temperature T_S cannot be pre-calculated as it depends on the changing composition of liquid. The steel composition varies and depends on the degree to which components are segregated due to the back diffusion and mass of the resulting precipitations. The back diffusion parameter α is a function of local solidification time t_s, which depends on a difference between liquidus and solidus temperatures.

3. Model of steel components segregation during solidification

The behavior of liquid steel components during its solidification has been described by, i.e. mathematical model created by Ueshima et al. [14-16]. This model accounts for the separation of solid particles in liquid during dendritic crystallization in directional heat removal conditions. Heat is removed vertically downwards. In such conditions liquid steel may coexist with phase γ, which originated from phase δ in a lower part of the sample. If the research focuses on the crystallization of phase δ, all alloy components will tend to gather in liquid steel. This means that the conditions for inclusion formation in the course of crystallization processes are favorable. The concentration C_{i0} of a given component „i" in the first part of the solidified phase is [17-18]:

$$C_{i0} = C_{iL}^{0} \cdot k_i^{\delta/L} \tag{18}$$

where:

C_{iL}^{0} – initial concentration of a component "i" in liquid phase,

$k_i^{\delta/L}$, $k_i^{\gamma/L}$ – solid/liquid phase (δ and γ) partition coefficient for "i" component.

During crystallization processes the liquid steel is enriched in component „i", and the successive portions of solid phase contain more and more of it. As a consequence the equilibrium concentration of component „i" in liquid phase decreases. The Ueshima model accounts for solidification of a selected layer, disposed perpendicular to the dendrite arm axis. While solidifying, the layer does not exchange the mass with environment. In the solidification process the temperature of a layer lowers from liquidus T_L to solidus temperature T_S. Time needed for a layer to solidify, i.e. local solidification time t_s, depends on the cooling rate P (K/min) [17-18]:

$$P = \frac{T_L - T_S}{t_s} \tag{19}$$

P – cooling rate [K/min].

The layer solidifies from the dendrite axis towards its edge. The diffusion of component „i" in liquid phase takes place fast enough to make the concentration of the component constant in a given moment of time. The diffusion of component „i" in solid phase is described by the Fick law [17-21]:

$$\frac{\partial C_i}{\partial t} = D \cdot \frac{\partial^2 C_i}{\partial x^2} \tag{20}$$

where C_i is concentration of "i" component in solid phase.

After introducing finite differences in the place of difference increases, the following is obtained for the analyzed case [17-18, 22-23]:

A. For a cell at the dendrite (n=1)

$$\frac{C_{i1}^{t} - C_{i1}^{t-\Delta t}}{\Delta t} = D \cdot \frac{C_{i2}^{t-\Delta t} - C_{i1}^{t-\Delta t}}{(\Delta x)^2} \tag{21}$$

B. For a cell in the solid phase (1<n<m)

$$\frac{C_{in}^{t} - C_{in}^{t-\Delta t}}{\Delta t} = D \cdot \frac{\left(C_{i(n+1)}^{t-\Delta t} - C_{in}^{t-\Delta t}\right) - \left(C_{in}^{t-\Delta t} - C_{i(n-1)}^{t-\Delta t}\right)}{(\Delta x)^2} \tag{22}$$

C. For a cell on the interface (n = m) at any point of time:

$$C_{im}^{t} = C_{iL}^{t} \cdot k_i^{\delta/L} \tag{23}$$

D. For every cell in the liquid (m<n<N) the concentration equal C_{iL}^{t}.

At each time step of computation the balance equation for every component is following:

$$N \cdot C_{iL}^{0} = \sum_{n=1}^{m} C_{in}^{t} + (N - m) \cdot C_{iL}^{t} \tag{24}$$

This equation enable one to calculate the component „i" at a moment t both in liquid phase (C_{iL}^{t}), and in a solidifying cell m (C_{im}^{t}):

$$C_{iL}^{t} = \frac{N \cdot C_{iL}^{0} - \sum_{n=1}^{m-1} C_{in}^{t-\Delta t} + F \cdot C_{i(m-1)}^{t-\Delta t}}{(N - m) + (1 - F) \cdot k_i^{\delta/L}} \tag{25}$$

$$C_{im}^{t} = \frac{C_{iL}^{t}}{k_i^{\delta/L}} \tag{26}$$

Parameter F determines given solidification conditions, i.e. given width of the cell, assumed time step Δt, local time of solidification t_s resulting from a difference of liquidus and solidus temperatures and the cooling rate P:

$$F = D \cdot \frac{\Delta t}{\Delta x^2} = \frac{4 \cdot D \cdot t_s}{L^2} \cdot N^2 \cdot \left[(f_s^{t})^2 - \left(f_s^{t-\Delta t}\right)^2 \right] \tag{27}$$

where f_s^{t} is a fraction of solid phase at a given point of time t.

Assumption was made that the solidification rate changes with solidification time parabolically [1]. For a given chemical composition of steel the liquidus temperature is T_L, and solidus temperature is T_S. On this basis the temperature corresponding to the contribution of solid phase f_s can be determined, i.e. location of cell $n = m$.

$$T = T_0 - \frac{T_0 - T_L}{1 - f_s \frac{T_L - T_s}{T_0 - T_s}} \tag{28}$$

T_0 – melting temperature of pure iron.

The microsegregation model allows to calculate the concentration of each component of the liquid phase at a given crystallization stage.

$$\sum_{n=1}^{N} C_{iL}^{0} = \sum_{n=1}^{m} C_{in}^{t} + (N - m) \cdot C_{iL}^{t} \cdot \sum_{n=1}^{m} C_{in}^{t} \cdot (N - n + 1) \tag{29}$$

C_{in}^{t} – consumption of a component to formation inclusions in the time interval from t-Δt to t.

Each calculation step should be followed by checking out whether respective dependences (13) and (14) are met, and take for the drop of concentration in the liquid phase balance (29).

4. Calculation of steel components concentration and inclusions formation in the solidifying steel ingot

Calculations of segregation and inclusions formation were made for two types of steel, the chemical composition of which is presented in Table 3.

TABLE 3
Chemical composition of steels chosen for the calculation of elements segregation and inclusions formation

Type of steel	Component of steel [mas.%]							
	C	Mn	Si	P	S	Ti	O	N
Steel 1	0.18	1.6	0.25	0.025	0.012	0.02	0.0005	0.005
Steel 2	0.24	1.1	0.37	0.04	0.04	0.15	0.0005	0.005

The liquidus and solidus temperatures for chemical composition of the steel were calculated from the equations [10]:

$$T_L = 1809 - \{100.3[\%C] - 22.4[\%C]^2 - 0.16 + 13.55[\%Si] - -0.64[\%Si]^2 + 5.82[\%Mn] + 0.3[\%Mn]^2 + 4.2[\%Cu]\} \quad (30)$$

$$T_S = 1809 - \{415.5[\%C] + 12.3[\%Si] + 6.8[\%Mn] + +124.5[\%P] + 183.9[\%S] + 4.1[\%Al]\} \quad (31)$$

TABLE 4
Calculated values of temperatures T_L and T_S [K]

Type of steel	T_L [K]	T_S [K]
Steel 1	1778	1718
Steel 2	1775	1685

The simulation was based on authors' computer software SEG_Stal, the calculations after the Ueshima model, which was adapted to the description of the segregation and inclusions formation in the ingot. The parameter L was assumed to be 110 mm. The crystallization with back diffusion was described with dependence (6). The activity of non-metallic phase components was obtained from dependence (3). The activity coefficients of particular steel components were determined from Wagner–Chipman equation. The first order activity parameters were assumed from [1, 4-5]. The activity of oxide phase components was established from expressions for a regular solution model. The calculation accounted for the activity parameters after Banya [1, 4-5]. The calculations were performed for the metallic/non-metallic interface equilibrium conditions with the equilibrium constants for inclusion formation reactions in liquid steel [1,7,8,11]. Figures 1-6 present a change of oxygen, nitrogen and titanium content as a result of segregation in steel 1 and 2 over the solidification process, at a cooling rate of 100 and 500 K/min. Figures 8-9 illustrate the process of TiN and Ti_2O_3 inclusions formation in steel 1 and 2 during solidification at a cooling rate of 100 and 500 K/min.

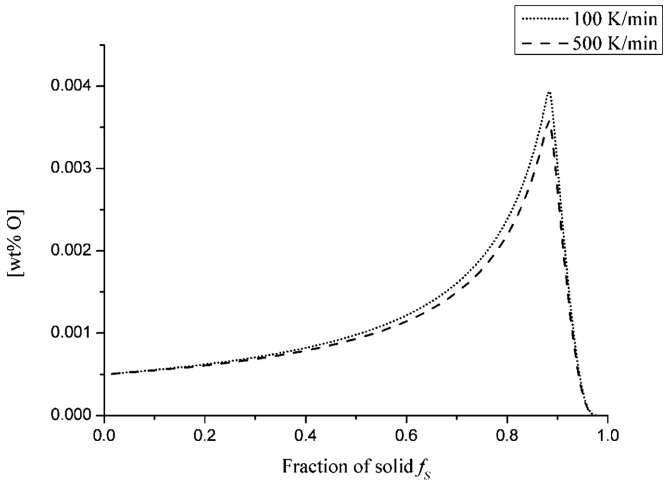

Fig. 1. Oxygen segregation during solidification of steel 1 at the cooling rate of 100 K/min and 500 K/min

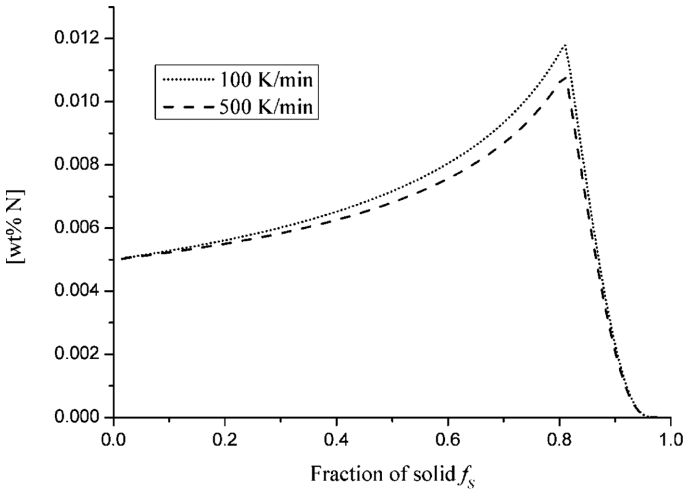

Fig. 2. Nitrogen segregation during solidification of steel 1 at the cooling rate of 100 K/min and 500K/min

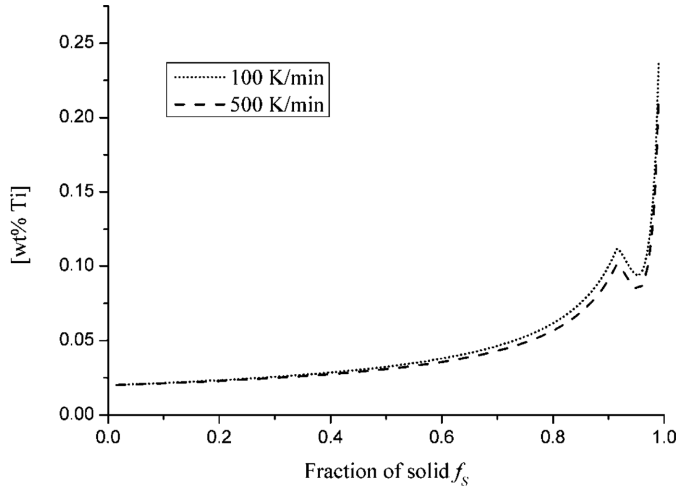

Fig. 3. Titanium segregation during solidification of steel 1 at the cooling rate of 100 K/min and 500 K/min

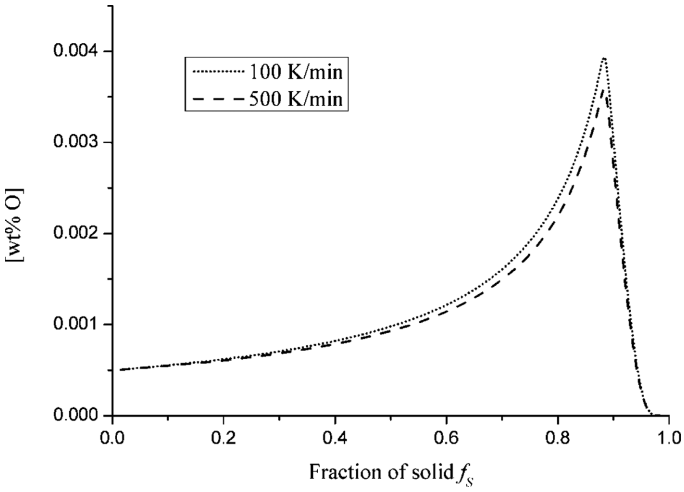

Fig. 4. Oxygen segregation during solidification of steel 2 at the cooling rate of 100 K/min and 500 K/min

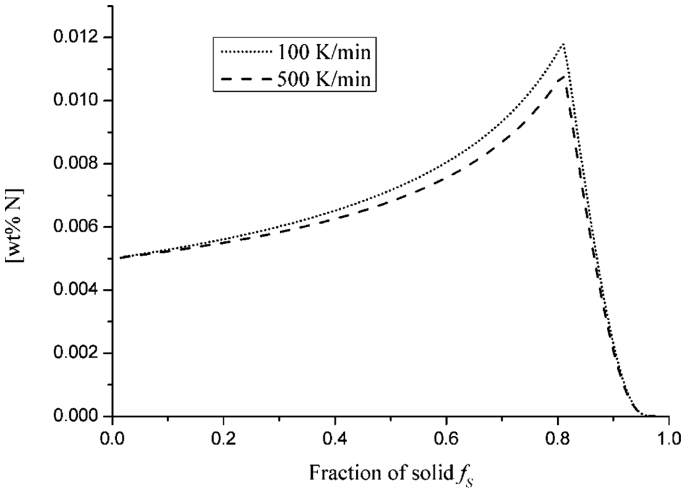

Fig. 5. Nitrogen segregation during solidification of steel 2 at the cooling rate of 100 K/min and 500 K/min

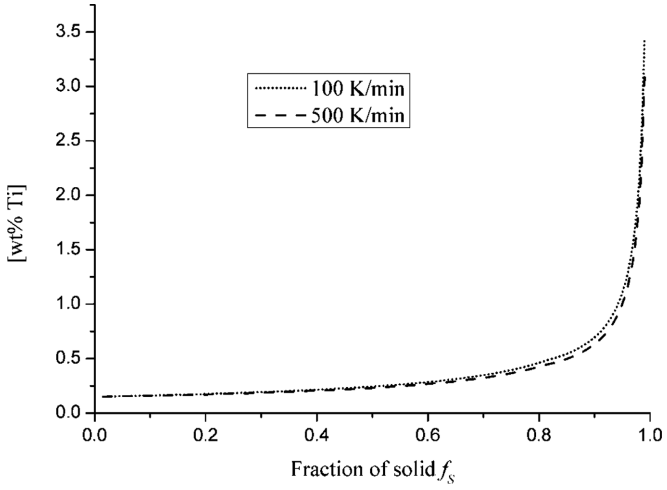

Fig. 6. Titanium segregation during solidification of steel 2 at the cooling rate of 100 K/min and 500 K/min

Oxygen and nitrogen have a low equilibrium interface division coefficient as compared to that of titanium. This means that the oxygen and nirtogen concentrations increase in liquid phase with the advancing solidification process. A break on the plots representing oxygen and nitrogen segregation in steel 1 (Fig. 1-2) and in steel 2 (Fig. 4-5) is indicative of inclusions formation. In the case of low titanium steel (steel 1) no break is visible on the segregation curve (Fig. 3), which means that titanium was consumed by oxygen and nitrogen in the process of non-metallic inclusions formation. In high titanium steel no. 2 no rapid break on the segregation plot was observed, signifying that after inclusions formation some amount of dissolved titanium was left out in liquid steel (Fig. 6). This effect was caused by the oxygen and nitrogen defficiency, due to which no further oxide and nitride precipitations could be formed.

The computer simulations revealed minimum differences in the segregation plots for titanium for cooling rates 100 K/min and 500 K/min. Bigger differences were visible in the segregation plots of oxygen and nitrogen, with biggest deviations between curves for nitrogen. At a cooling rate of 100 K/min most of the elements remain in liquid steel.

Figures 7 and 8 illustrate the process of TiN and Ti_2O_3 inclusions formation in steel 1 and 2 during solidification, at a cooling rate of 100 and 500 K/min.

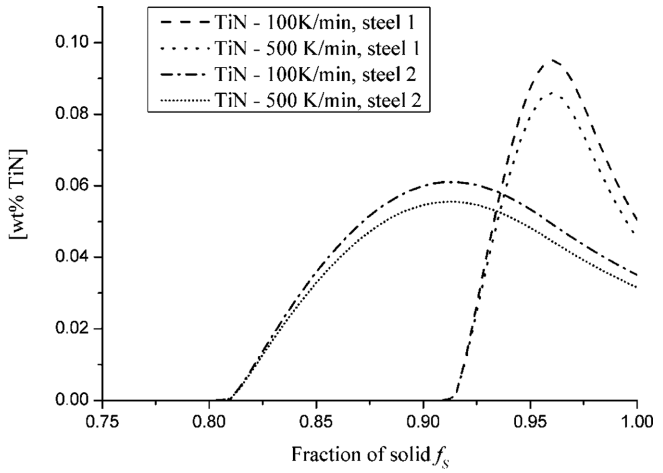

Fig. 7. Formation of TiN particles during solidification of steel 1 and 2 at the cooling rate of 100 K/min and 500 K/min

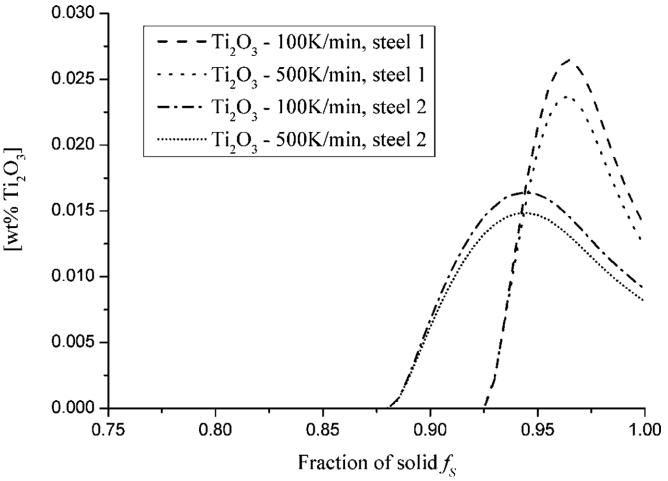

Fig. 8. Formation of Ti_2O_3 particles during solidification of steel 1 and 2 at the cooling rate of 100 K/min and 500 K/min

The calculations for low- and high-titanium steels revealed that TiN inclusions were formed at an earlier stage of

solidification than Ti_2O_3, being a result of the concentration of the components in the liquid steel and actual value of the real and equilibrium solubility product of oxide and nitride precipitates. TiN particles were formed at the final stage of solidification process, when the solid phase fraction equaled to 0.9 for steel 1 and about 0.8 for steel 2. This process continued till the moment the last portion of liquid steel solidified. Most of the TiN inclusions were formed with the participation of solid phase 0.97 for steel 1 and 0.9 for steel 2. Ti_2O_3 particles were formed with the participation of solid phase 0.925 for steel 1 and 0.87 for steel 2, respectively. The most of the titanium oxide precipitates were formed with the participation of solid phase 0.96 for steel 1 and 0.93 for steel 2. The computer simulations also showed that both in the case of low- and high-titanium steels more inclusions were formed at a lower solidification rate, i.e. 100 K/min. This effect was caused by the fact that back diffusion in the process of elements segregation during solidification of analyzed steels was accounted for Wołczyński equation.

5. Concluding remarks

The simulation results of secondary precipitations formation during solidification of low- and high-titanium steels with the use of a modified Ueshima model and simplex optimization method revealed that the main parameter deciding about the formation of TiN and Ti_2O_3 inclusions was the percentage of elements making up both compounds. Calculations were focused on the non-metallic inclusions formation in the steel solidification process, without accounting for the primary inclusions formation. Based on the results of calculations performed with software SEG_Stal the approximate distribution of secondary inclusions formed in steel during its solidification could be obtained. The results revealed that more precipitations were formed at a lower rate of cooling, and the differences in the amount of the resulting TiN and Ti_2O_3 inclusions for both rates 100 K/min and 500 K/min were minimal. It was also observed that TiN inclusion in steel 1 were formed at the same participation of solid phase, regardless the solidification rate. An analogous effect was observed for steel 2. In the case of Ti_2O_3 precipitations formation in steels 1 and 2 a similar trend was noted. The calculations did not account for such effects as outflow of inclusions and their assimilation to slag or interaction of formed particles with the solidification front. This would, however, give a fuller picture of distribution of inclusions in ingots of analyzed steels.

Acknowledgements

This study was solved within the framework of the project Reg. **No. 11.11.170.318** task 1 at financial support of Ministry of Science and Higher Education Republic of Poland.

REFERENCES

[1] D. Kalisz, Thermodynamic Characteristics of the Non-metallic Phase Formation in the Liquid Steel, Wydawnictwo Naukowe Akapit, Krakow (2013).

[2] F. Ishikawa, T. Takahashi, T. Ochi, Intergranular ferrite nucleation in medium – carbon vanadium Steels, Met. Materials Trans. A **25A**, 929-936 (1994).

[3] J.M. Gregg, H.K. Bhadeshia, Solid State Nucleation of Acxicular Ferrite on Minerals Added to Molten Steel, Acta Mater. **45**, 739-748 (1979).

[4] J. Iwanciw, D. Podorska, J. Wypartowicz, Calculations of Oxide Inclusions Composition in Steel Deoxidized with Mn, Si and Ti, Arch. Metal. And Mat. **53**, 3, 635-644 (2011).

[5] J. Iwanciw, D. Podorska, J. Wypartowicz, Modeling of Oxide Precipitates Chemical Composition During Steel Deoxidation, Arch. Metal. And Mat. **53**, 4, 999-1005 (2011).

[6] M. Holtzer, Metallurgy and Foundry Processes of Iron Alloys. Physicochemical Fundamentals, Wydawnictwo Naukowe PWN (2013).

[7] Z. Morita, T. Tanaka, N. Sano, Equilibria of Nitride Forming Reactions in Liquid Iron Alloys, Met. Trans. B, **18B**, (1987).

[8] Z. Liu, K. Gu, K. Cai, Mathematical Model of Sulfide Precipitation on Oxides During Solidification of Fe-Si Alloy, ISIJ Int. **42**, 950-957 (2002).

[9] M.A. Van Ende, M. Guo, R. Dekkers, M. Burty, J. Van Dyck, P.T. Jones, B. Blanpain, P. Wollants, Formation and Evolution of Al-Ti Oxide Inclusions During Secondary Steel Refining, ISIJ Int. **49**, 1133-1140 (2009).

[10] M. Suzuki, R. Yamaguchi, K. Kajioka, Inclusion Particle Growth During Solidification of Stainless Steel, ISIJ Int. **41**, 247-256 (2001).

[11] Z. Ma, D. Janke, Characteristic of Oxide Precipitation and Growth during Solidification of Deoxidized Steel, ISIJ Int. **38**, 46-52 (1998).

[12] W. Wołczyński, Effect of the Back – Diffusion onto Doublet Structure Formation and Solute Redistribution Within Alloys Solidyfying Directionaly, With or Without Convection, Polish Academy of Sciences, Institute of Metallurgy and Materials Science, Krakow (2002).

[13] J. Lei, Z. Xue, Y. Jiang, J. Zhang, T. Zhu, Study of TiN Precipitation During Solidification for Hypereutectoid Tire Cord Steel, Metallurgia Int. **17**, (2012).

[14] Z. Liu, J. Wei, K. Cai, Coupled Mathematical Model of Microsegregation and Inclusions Precipitation during Solidification of Silicon Steel, ISIJ Int. **42**, 958-963 (2002).

[15] Y. Ueshima, Y. Sawada, S. Mizoguchi, H. Kajioka, Precipitation Behavior of MnS During δ/γ Transformation in Fe-Si Alloy, Mert. Trans. **20A**, 1375-1383 (1989).

[16] T. Matsumiya, H. Kajioka, S. Mizoguchi, Y. Ueshima, Mathematical Analysis of Segregation in Continuously Cast Slabs, Trans. ISIJ 24 (1984).

[17] J. Lelito, P.L. Żak, A.A. Shirzadi, A.L. Greer, W.K. Krajewski, J.S. Suchy, K. Haberl, P. Schumacher, Effect of SiC Reinforcement Particles on the Grain Denisity in a Magnesium Based Metal – Matrix Composite: Modelling and Experiment, Acta Materialia **60**, 2950-2958 (2012).

[18] J. Lelito, P.L. Żak, A.L. Greer, J.S. Suchy, W.K. Krajewski, B. Gracz, M. Szucki, A.A. Shirzadi, Crystallization model of magnesium primary chase in the AZ91/SiC composite, Composites Part B: Engineering **43**, 3306-3309 (2012).

[19] J. Lelito, P.L. Żak, J.S. Suchy, W.K. Krajewski, A.L. Greer, P. Dartak, Experimental Determination of Grain Denisity Function of AZ91/SiC Composite with Different Mass Fraction of SiC and Undercoolings Using Heterogeneous Model, China Foundry, 8 (1), p. 101-106 (2011).

[20] W. K a p t u r k i e w i c z, E. F r a ś, A.A. B u r b e l k o, Computer Simulation of the Austenitizing Process in Cast Iron with Pearlitic Matrix, Materials Science and Engineering A: Structural Materials: Proporties, Microstructure and Processing **413-414**, 352-357 (2005).

[21] J.S. S u c h y, J. L e l i t o, B. G r a c z, P.L. Ż a k, H. K r a w i e c, Modelling of Composite Crystallization, China Foundry **9** (2), 184-188 (2012).

[22] E. M a j c h r z a k, R. S z o p a, Simulation of Heat and Mass Transfer in Domain of Solidifying Binary Alloy, Archives of Metallurgy **43** (4), 341-351 (1998).

[23] R. H a w r a n e k, J. L e l i t o, J.S. S u c h y, P.L. Ż a k, The Simulation of Liquid Cast Iron Flow Through the Casting System with Filter, Archives of Metallurgy and Materials **54** (2), 351-358 (2009).

Received: 20 January 2014.